Three-dimensional massless Dirac fermions in carbon schwarzites

Aurélien Lherbier,[1,][*] Humberto Terrones,[2] and Jean-Christophe Charlier[1]

[1]*Université catholique de Louvain, Institute of Condensed Matter and Nanosciences, Chemin des étoiles 8, 1348 Louvain-la-Neuve, Belgium*
[2]*Department of Physics, Applied Physics and Astronomy, Rensselaer Polytechnic Institute, Troy 11248, New York, USA*

The discovery of gapless linear energy dispersion in low-dimensional carbon-based nanostructures had a tremendous impact on conventional condensed-matter physics by imposing relativistic physics in the electronic properties of these nanosystems. Indeed, the electrons in graphene [two-dimensional (2D)] and carbon nanotubes [one-dimensional (1D)] behave like pseudorelativistic massless particles (Dirac fermions) as described by the crossing of linearly dispersive electronic bands, also called the Dirac cone. The presence of Dirac cones is not restricted to 1D or 2D nanostructures and has recently been observed in several more complex 3D materials. Here, using density functional theory and tight-binding approaches, we predict the presence of a Dirac cone in a 3D carbon-based material. Indeed, our simulations reveal a linear band crossing merging in a point forming a Dirac (hyper)cone for a large gyroidal schwarzite structure. Such a specific linear dispersion relation as reported in this 3D negatively curved sp^2-bonded carbon allotrope is believed to be a direct consequence of the Dirac cone present in 2D graphene. The corresponding charge carriers are thus expected to behave as 3D massless Dirac fermions. Therefore, we expect this prediction to stimulate the experimental synthesis of such fascinating 3D bulk carbon allotropes, which are a remarkable playground to investigate relativistic physics of these exotic fermions.

I. INTRODUCTION

Massless electrons for which the energy dispersion relation is linear are not frequently observed in the electronic structures of materials. It is even more exceptional when these linear electronic bands are merged into a crossing point, where the Fermi surface is then reduced to a single spot. Such electrons can locally be described as massless Dirac fermions whose related physics is fascinating and different than that for conventional massive fermions. In modern condensed-matter physics, such pseudorelativistic electrons occupy a more and more dominant position because their unique properties, such as ultrahigh mobility and the possibility of Klein tunneling [1], motivate new paradigms in electronics and hence potential disrupting technology. Although the first prediction of a linear energy dispersion of electrons in graphene goes back to 1947 with the seminal paper of Wallace [2], it is only with carbon nanotubes and, even more significant, with the advent of graphene [3,4] demonstrating uncommon phenomena such as anomalous quantum Hall effects [5,6] that massless Dirac fermions became genuinely popular in condensed-matter physics. Now, not only Dirac fermions are in the spotlight. More and more exotic particles which used to be popular almost solely in the field of high-energy physics are now being included in the study of condensed-matter physics. In recent years, considerable efforts have been made to realize the experimental synthesis of new materials that could contain an unusual class of fermions such as Dirac electrons [7–14] or Majorana electrons [15,16].

While the existence of Dirac fermions in low-dimensional systems had been well established, evidence of bulk massless Dirac fermions in three-dimensional (3D) materials had still been missing. Their presence has recently been experimentally

detected through angle-resolved photoemission spectroscopy (ARPES) measurements in Na_3Bi [10] and in Cd_3As_2 [11,12] and through the anomalous quantum Hall effect in HgCdTe [13]. However, although massless Dirac fermions are present in one-dimensional (1D) and two-dimensional (2D) sp^2 carbon materials, namely, carbon nanotubes and graphene, to date, the presence of bulk massless Dirac fermions in a 3D carbon-based system has not been reported yet. The goal of the present paper is to predict the possibility to observe such bulk massless Dirac electrons in a 3D lattice of sp^2-bonded carbon atoms whose atomic structure is a gyroidal schwarzite.

The schwarzite structures come from the decoration of triply periodic minimal surfaces (TPMS); thus they exhibit high surface areas and negative Gaussian curvature due to the presence of carbon-membered rings with more than six atoms [17]. Carbon-based schwarzites were naturally first suggested as 3D counterparts of the zero-dimensional (0D) fullerenes, which, in contrast, have a positive Gaussian curvature through the presence of pentagonal rings of carbon. Although density functional theory (DFT) predicts that several types of schwarzites are more stable than C_{60} [18], such 3D carbon allotropic forms have not yet been experimentally synthesized and therefore remain largely unexplored compared to other more fashionable carbon nanostructures. Although schwarzites remain elusive, recent advances in templated nanocarbons [19,20] in combination with new liquid exfoliation techniques for obtaining graphene and monolayer transition-metal dichalcogenides [21] indicate the right strategy to follow in order to get closer than ever to the mysterious schwarzites. Conjectural materials often need outstanding properties to boost motivation towards their experimental synthesis. Schwarzites have already been considered good candidates for electrodes in the next generation of alkali-ion batteries and supercapacitors [22] because their nanoscale sponge structures offer an extreme bulk-surface ratio. The present theoretical prediction of massless Dirac electrons in

*aurelien.lherbier@uclouvain.be

such 3D carbon surfaces will certainly enhance the interest in these schwarzite structures and graphene sponges.

II. STRUCTURAL PROPERTIES

A. Atomic structure

Large gyroidal schwarzites basically consist of bent graphene layers curved in a particular and periodical way in which two intertwined labyrinths, one the mirror image of the other, are formed. Schwarzites are therefore essentially 3D space partitioners made out of bent graphene layers. As for fullerenes, non-hexagonal-membered rings have to be introduced in the sp^2-bonded carbon surface to accommodate the curvature present in schwarzites. Moreover, the number of these non-hexagonal-membered rings has to satisfy the following expression extracted from the Euler theorem: $2n_4 + n_5 - n_7 - 2n_8 = 12(1 - g)$, where n_i are integers representing the number of polygons composed of i vertices (e.g., n_7 is the number of heptagons) and g is the genus or number of handles in the structure (a topological invariant). In the case of schwarzites, g is the genus per primitive cell. Note that the number of hexagons n_6 is thus irrelevant since they do not contribute to the curvature of the system. The present investigated gyroidal schwarzite corresponds to $g = 3$ per primitive cell exhibiting 12 octagonal rings ($n_8 = 12$). Consequently, the curvature is only induced by these 12 octagons present at the saddle-node points of the structure. Since schwarzites are periodic crystals of sp^2 carbon, their symmetry is related to the symmetry of the associated TPMS. In the case of gyroidal (G) TPMS or G schwarzites, the space group is $Ia\bar{3}d$ with a bcc Bravais lattice. In our particular case the primitive cell contains 768 carbon atoms (1536 atoms per conventional cubic cell) [see Fig. 1(a)] and possesses a surface area of 2670 m^2/g, close to that of graphene, which is around 2675 m^2/g [23]. The atomic coordinates of this large G-schwarzite structure were obtained by inflating, i.e., adding hexagonal rings of carbon between octagons, to the model of the G-8-bal structure given in Ref. [24].

B. Geometry optimization

DFT-based calculations have been performed to relax both the atomic positions and the cell volume of this G-schwarzite structure. The DFT calculations were conducted using the SIESTA package [25] using the Perdew-Burke-Ernzerhof (PBE) generalized gradient approximation (GGA) functional [26]. Core electrons were accounted for through the use of Troullier-Martins pseudopotentials [27]. The valence electron wave functions were expanded in a double-ζ polarized (DZP) basis set of finite-range numerical pseudoatomic orbitals [28]. The density was self-consistently calculated using a mesh cutoff of 250 Ry and a $2 \times 2 \times 2$ Monkhorst-Pack k-point grid [29]. The atomic positions were optimized for a fixed lattice parameter by relaxing the forces until a maximum tolerance criterion of 0.01 eV/Å was reached. The bulk modulus B_0 was computed using this relaxation procedure performed for different lattice parameters [$b = a\sqrt{3}/2$, where b is the primitive lattice parameter indicated in Fig. 1(a) and a is the conventional cubic lattice parameter] and was predicted to be in the range of 40 GPa [Fig. 1(b)]. This is a typical value for glassy materials
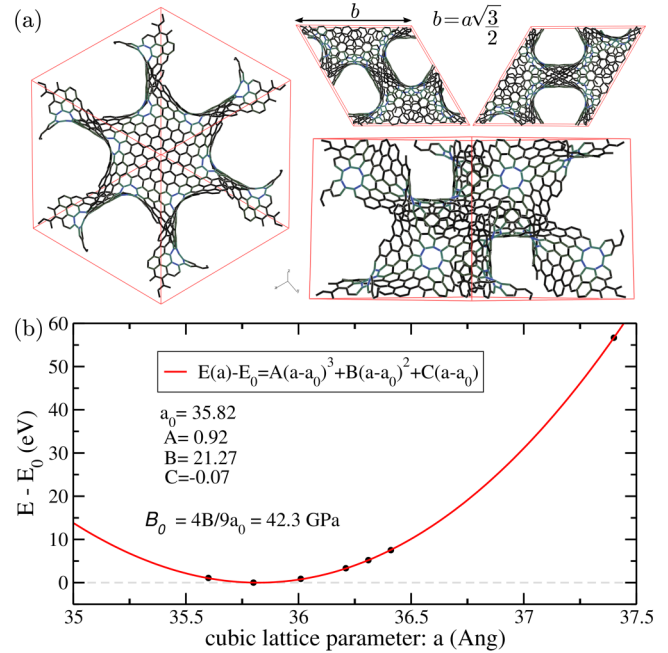
FIG. 1. (Color online) (a) Different view angles of the atomic structure of the gyroidal (G) schwarzite: the [111] orientation (left panel), the [100] and [010] orientation (top right panels), and the [110] orientation (bottom right panel). The system contains 768 carbon atoms in the present primitive unit cell (bcc cell with lattice parameter b indicated by an arrow). Carbon bonds are colored from black to blue with increasing length, highlighting the presence of the 12 octagons. (b) Total energy dependence on the cubic lattice parameter a. The equilibrium lattice parameter minimizing the total energy is estimated to be $a_0 = 35.82$ Å using a polynomial fit. The corresponding bulk modulus is $B_0 \sim 40$ GPa.

and is thus much lower than that for incompressible materials, which is in agreement with the flexible sponge structure of schwarzite.

III. ELECTRONIC PROPERTIES

A. Band structure and Dirac fermions

From the optimized atomic structure, the *ab initio* band structure and density of states (DOS) have been computed and are depicted in Fig. 2(a) (black lines). The band structure is calculated along the usual high symmetry points of the bcc Brillouin zone, i.e., a Γ-H-N-Γ-P-H-N-P path. The DOS is obtained from a self-consistent calculation using a $6 \times 6 \times 6$ k-point grid and a smearing factor of 25 meV. Linearly dispersive bands are observed around the high-symmetry point P, i.e., at the corner of the Brillouin zone. Two crossing points related to these linear dispersions are located at energies of about $+0.5$ eV (above the Fermi energy E_F) and at -0.35 eV (below E_F) in the electron and hole regions, respectively. Around these Dirac points, energy windows of a few tenths of eV are free of other bands, reducing the Fermi surface to a single spot exactly at the Dirac energy E_D. However, the latter acquires a spherical shape whose radius increases linearly with energy when moving away from these Dirac points [Fig. 2(b)].
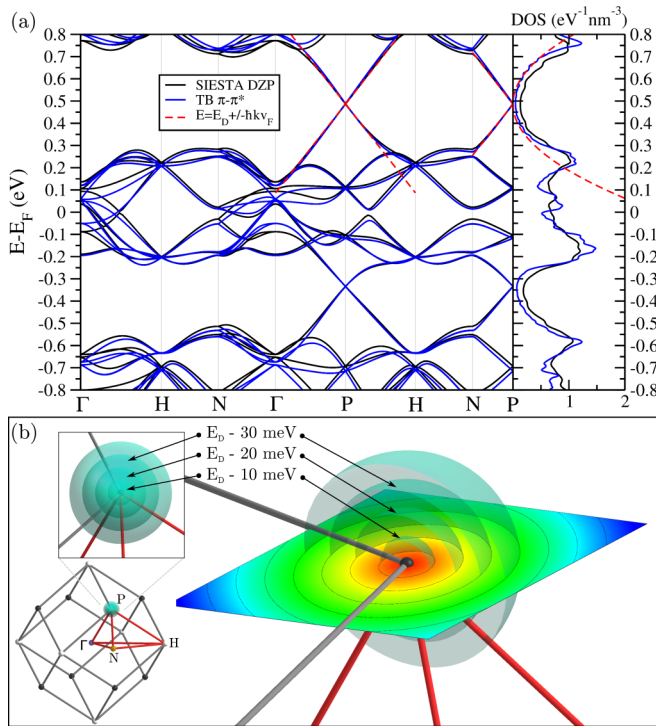
FIG. 2. (Color online) (a) The DFT (black lines) and TB (blue lines) band structures are calculated along the conventional Γ-H-N-Γ-P-H-N-P path. Two Dirac points are observed at the P point in both the valence and conduction sides ($E = -0.35$ eV and $E = +0.5$ eV). The analytical Dirac equation $E = E_D \pm \hbar k v_F$ is used to plot the linear dispersion around the Dirac point for electrons (red dashed lines). The corresponding densities of states are represented in the right panel. (b) Brillouin zone (bottom left) and 3D energy isocurves of the 4D Dirac hypercone. At the Dirac point, located at the corner of the Brillouin zone, the Fermi surface reduces to a spot and displays a perfect spherical shape when moving away from the Dirac point energy E_D. The central image shows a magnification of the top left image together with a cutting plane with a color map of the energy variation (from red at $E = E_D$ to blue for $E = E_D + 70$ meV. The radius of this Fermi sphere increases linearly with the energy.

It has to be noted that the electron Dirac (hyper)cone [it is a four-dimensional (4D) object, i.e., the energy as a function of the three directions in k space] is very isotropic and symmetric in a fairly large energy range of $\sim$400 meV. It is also worth mentioning that the Dirac hypercone at a given energy is fourfold degenerate. The first twofold degeneracy has its origin in a valley degeneracy, as in graphene, coming from the two inequivalent P points (P and $P' = -P$) over the eight-corner highly symmetric points of the bcc Brillouin zone [black dots in the left panel of Fig. 2(b)]. This valley degeneracy directly creates two copies of the Dirac hypercone. The second two-fold degeneracy is internal to a given Dirac hypercone since two superimposed bands coexist [indistinguishable in Fig. 2(a)]. Using this order of degeneracy and the Dirac linear energy dispersion $E = E_D \pm \hbar k v_F$ [dashed red lines in Fig. 2(a)], an analytical formula for the DOS ρ can be established, which is $\rho = \frac{4}{2\pi^2} \frac{(E-E_D)^2}{(\hbar v_F)^3}$ (spin degeneracy not included). Hence, the DOS for the massless charge carriers in schwarzite is comparable to the DOS of photons but with a

higher degree of degeneracy [dashed red curve in Fig. 2(a)]. The speed of light c is replaced here by the Fermi velocity v_F, which is found to be 2.5 times smaller than in 2D graphene (i.e., $\sim$4 $\times$ 10^5 m s^{-1} $\sim$ c/750).

Finally, note that the presence of the Dirac hypercone is robust against volume expansion. While the band structure changes around the Fermi level for the non-fully-relaxed geometry [30], the Dirac hypercones are still preserved for an $\sim$4.5% expansion of the cell vector length, corresponding to the largest cell volume in Fig. 1(b).

The present G-schwarzite band structure does not exhibit any band gap at the Fermi level and possesses an overall electron-hole symmetry, reminiscent of the 2D graphene π-π^* electronic structure. For this reason and adding the fact that such a large G schwarzite resembles a twisted graphene layer with octagons, a simple one-orbital p_z tight-binding (TB) model was expected to be sufficient to reproduce its electronic structure. A first-nearest-neighbor π-π^* TB model (not shown here) already provides a good match but fails to reproduce accurate details at the Fermi level or to introduce an artificial band gap as well as fully symmetric conduction- and valence-band structures. However, better agreement is obtained with a semiempirical distance-dependent π-π^* TB model [31] [blue lines in Fig. 2(a)]. In this model, the distance-dependent hopping term reads $\gamma(d) = \gamma_0 e^{-3.37(\frac{d}{d_{CC}}-1)}$, where $\gamma_0 = 2.8$ eV and $d_{CC} = 1.41$ Å. A cutoff distance of 3.1 Å surrounding the third-nearest neighbors was applied. For the fully relaxed schwarzite structure, the octagons encounter a stronger distortion. This is accounted for in the present TB model by modifying the p_z orbital on-site energy ($\delta\epsilon_{p_z} = -0.5$ eV), and the hopping energy ($\delta\gamma = +0.15$ eV) for carbon atoms belonging to an octagon. The only deficiencies of this semiempirical model can be observed around the Γ point (at $E = +0.1$ eV and $E = -0.1$ eV), where the TB bands are not well positioned in energy compared to the DFT bands. These two particular pairs of bands are more sensitive to the on-site and hopping energies of the carbon atoms involved in the octagons.

Using this TB model, the DOS in Fig. 2(a) was obtained with a 15 $\times$ 15 $\times$ 15 k-point grid and a smearing factor of 10 meV. The energy isosurfaces depicted in Fig. 2(b) were obtained using this TB model and by computing eigenenergies in a cubic mesh of $\sim$36 000 k points.

B. Doping and Fermi-level shift

The Dirac hypercones are well separated from the rest of the other bands (especially for electrons), offering the possibility to observe independently the properties of the corresponding massless 3D Dirac fermions without them being mixed with other massive fermions. Also, the fact that the present Dirac hypercones are fully isotropic and symmetric is rather unique, to the best of our knowledge.

However, the Dirac hypercones are, unfortunately, not lying at the Fermi energy. Different suggestions could be proposed to shift the Fermi level at the Dirac point. For instance, a nonperturbative approach would be to contact and gate the system and fill or deplete it with charge carriers by applying an adequate gate voltage. However, in typical conditions, the required gate capacitance to move Fermi energy of such an
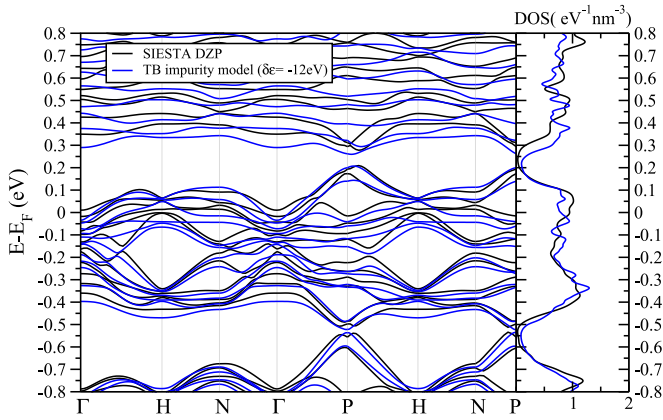
FIG. 3. (Color online) The DFT band structures and DOS of a 0.8% N-doped schwarzite (black lines). A simplified impurity TB model ($\delta\epsilon = -12$ eV) reproduces the main features of the N dopants (blue lines).

FIG. 4. (Color online) TB band structures and DOS for the pristine and two impurity models ($\delta\epsilon = -1, -2$ eV) for which the on-site energy terms of carbon atoms belonging to the octagons are modified (12.5%).

amount might be too high. Doping with nitrogen or boron could also be an interesting and natural route. Such chemical doping would easily induce a shift of the Fermi-level position. However, *ab initio* calculations of a 0.8% N-doped schwarzite (six N atoms in substitution, randomly chosen) indicate that such chemical doping is too intrusive (Fig. 3, black lines). The Dirac points are split and shifted away from the high-symmetry path, giving rise to the small apparent band gap. Moreover, the hypercone internal degeneracy is lifted, and the two superimposed Dirac cones are now easily distinguishable. Since 1.6% of N doping would be needed to bring E_F exactly to the Dirac point, such a chemical doping is probably not an appropriate strategy. As an alternative to the chemical and electrostatic doping proposed above, the charge transfer occurring through π-π stacking of physisorbed molecules, for instance, might provide soft doping, thus satisfying a rigid-band-model approach. Since schwarzite offers a large surface area, this could be an interesting route.

Using a simplified impurity model within the TB approach, realized by shifting the on-site energy of the p_z orbital of the impurity, the main features of the N-doped G-schwarzite band structure can be reproduced (blue lines in Fig. 3). Although this impurity model is oversimplified, it allows one to investigate other doping situations easily. An interesting solution is obtained by positioning impurities only at the octagonal carbon rings. While the number of modified carbon atoms reaches the high concentration of 12.5%, the corresponding band structure preserves the presence of the Dirac cone and Dirac nodal point in the conduction bands (Fig. 4). In contrast, the valence-band structure is strongly modified, and the valence Dirac cone rapidly disappears upon this specific doping. Because of this high concentration of modified carbon atoms, even a small charge transfer to each carbon atom would be sufficient to shift E_F towards E_D. Although obtained from a simplified TB impurity model, this result suggests that doping the octagonal ring sites with, for instance, metal adatoms such as Pt or Ti [32] or Li [33] in the hollow position, i.e., at the center of the octagons, could be an interesting route.

As a proof of concept, the case of Li has been calculated with the DFT approach. The Li atoms are initially placed
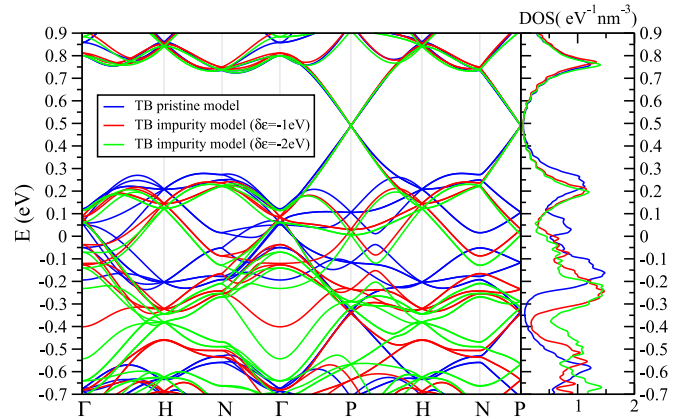
at the center of the octagons (12 Li atoms total), and their positions are optimized under the conjugated-gradient approach, keeping all carbon positions fixed. Different views of the final structure geometry are given in Fig. 5(a), showing that Li are alternatively positioned slightly *below* and *above* the surface. The corresponding band structure is depicted in Fig. 5(b). The Fermi energy is now lying very close to the Dirac point. Furthermore, the splitting and degeneracy lifting are much weaker than in the case of the random nitrogen-doping case, demonstrating that this particular doping at octagons should be preferred to better preserve the Dirac fermions. Although the present results tend to demonstrate that these Dirac cones undergo important deformations with symmetry
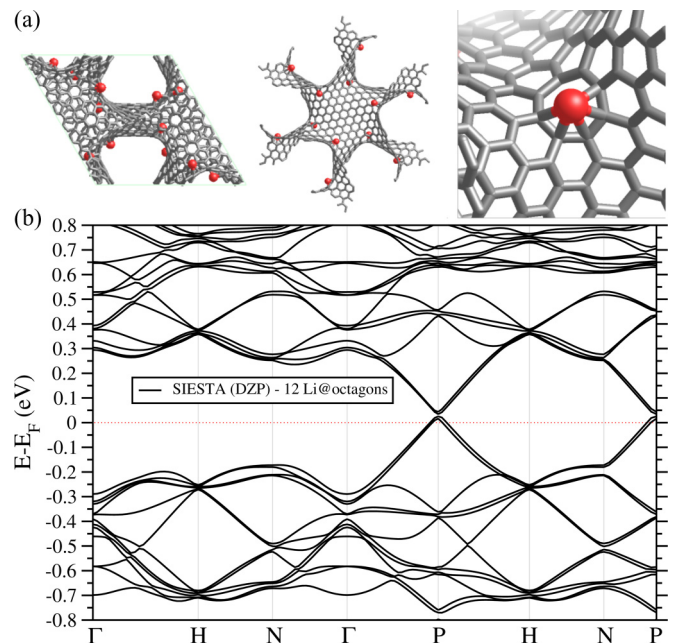
FIG. 5. (Color online) (a) Different view angles of the atomic structure of a Li-doped G schwarzite (12 Li atoms at the octagonal sites). (b) DFT band structure of the Li-doped G schwarzite. The Fermi level lies just below the Dirac point.

breaking, Fig. 5 illustrates a possible solution for correctly moving the Fermi energy towards the Dirac point. Finally, it is worth mentioning that other carbon schwarzite structures could host Dirac fermions, possibly lying directly at the Fermi energy and/or being more robust against symmetry breaking.

IV. DISCUSSION

The true connection between graphene's Dirac cone and the present Dirac hypercone remains to be clarified. However, several hypotheses can be mentioned. The first hypothesis is that the present schwarzite structure is sufficiently large to avoid high strain induced by curvature and thus does not destroy the resemblance to graphene's Dirac cone. This is consistent with the sp^2 hybridization of carbon, confirmed by the π-π^* character of electronic bands around the Fermi energy and the possibility to reproduce them with a one-atomic-orbital TB model. Moreover, if linear band crossings were frequently observed in previously computed band structures of smaller schwarzites [34], no isolated Dirac cones have been detected. The second hypothesis is that the present schwarzite containing only even-membered rings (octagons and hexagons) preserves the existence of two sublattices, hence allowing the wave function to eventually conserve a spinorial component linked to the bipartite nature of the honeycomb lattice. The third hypothesis is to consider the structure as a larger crystalline network whose nodes are centered at the octagons. Indeed, molecular crystalline structures have been shown to host Dirac cones, at least in planar (Euclidean) systems such as in graphyne [9] and in other pseudographenic systems such as molecular graphene assemblies [35]. Although the surface is non-Euclidean here, a hexagonal patch can still be formed where each octagon placed at the vertices is separated by a strip of three benzene rings from the four nearest-neighbor octagons [see left panel of Fig. 1(a)].

V. CONCLUSION

Carbon is a highly versatile chemical element accepting different atomic orbital hybridizations, allowing a large variety of carbon-based materials with outstanding properties. Carbon allotropes can be found in all dimensions (0D fullerenes, 1D carbon nanotubes and nanoribbons, 2D graphene layers, 3D graphite and diamond). Although known as a 3D counterpart of fullerenes since the early 1990s [17,18,34,36], schwarzite structures have received increasing attention in recent years due to the recent interest in finding a graphene foam [37–39]. As reported herein, the possible presence of 3D isotropic massless Dirac fermions represents another strong reason to have a closer look at schwarzite-related systems. While the exact conditions for the existence of such Dirac hypercones in schwarzites are still unclear, the effect on the electronic transport properties should be investigated. As for graphene, the Klein tunneling paradox is expected to be observed in this schwarzite structure. A sizable linear quantum magnetoresistance has recently been predicted for 3D massless Dirac fermions [40], and this prediction needs to be confirmed in schwarzites, along with other transport properties. Schwarzites are distinguished from the other carbon compounds by the fact that they belong to a non-Euclidean geometry with a negative Gaussian curvature (the hyperbolic geometry). Thus, including a new type of geometry certainly might result in materials with novel and fascinating properties, such as the reported 3D massless fermions, which could open new avenues in electronics for carbon-based materials.

[1] M. I. Katsnelson, K. S. Novoselov, and A. K. Geim, Nat. Phys. **2**, 620 (2006).

[2] P. R. Wallace, Phys. Rev. **71**, 622 (1947).

[3] A. K. Geim and K. S. Novoselov, Nat. Mater. **6**, 183 (2007).

[4] K. S. Novoselov, A. K. Geim, S. V. Morozov, D. Jiang, Y. Zhang, S. V. Dubonos, I. V. Grigorieva, and A. A. Firsov, Science **306**, 666 (2004).

[5] K. S. Novoselov, A. K. Geim, S. V. Morozov, M. I. Katsnelson, I. V. Grigorieva, S. V. Dubonos, and A. A. Firsov, Nature (London) **438**, 197 (2005).

[6] K. I. Bolotin, F. Ghahari, H. L. Stormer, and P. Kim, Nature (London) **462**, 196 (2009).

[7] S. M. Young, S. Zaheer, J. C. Y. Teo, C. L. Kane, E. J. Mele, and A. M. Rappe, Phys. Rev. Lett. **108**, 140405 (2012).

[8] Z. Wang, Y. Sun, X.-Q. Chen, C. Franchini, G. Xu, H. Weng, X. Dai, and Z. Fang, Phys. Rev. B **85**, 195320 (2012).

[9] D. Malko, C. Neiss, F. Viñes, and A. Görling, Phys. Rev. Lett. **108**, 086804 (2012).

[10] Z. K. Liu, B. Zhou, Y. Zhang, Z. J. Wang, H. M. Weng, D. Prabhakaran, S.-K. Mo, Z. X. Shen, Z. Fang, X. Dai, Z. Hussain, and Y. L. Chen, Science **343**, 864 (2014).

[11] M. Neupane, S.-Y. Xu, R. Sankar, N. Alidoust, G. Bian, C. Liu, I. Belopolski, T.-R. Chang, H.-T. Jeng, H. Lin, A. Bansil, F. Chou, and M. Z. Hasan, Nat. Commun. **5**, 3786 (2014).

[12] S. Borisenko, Q. Gibson, D. Evtushinsky, V. Zabolotnyy, B. Buechner, and R. J. Cava, Phys. Rev. Lett. **113**, 027603 (2014).

[13] M. Orlita, D. M. Basko, M. S. Zholudev, F. Teppe, W. Knap, V. I. Gavrilenko, N. N. Mikhailov, S. A. Dvoretskii, P. Neugebauer, C. Faugeras, A.-L. Barra, G. Martinez, and M. Potemski, Nat. Phys. **10**, 233 (2014).

[14] X. Wan, A. M. Turner, A. Vishwanath, and S. Y. Savrasov, Phys. Rev. B **83**, 205101 (2011).

[15] M. Franz, Physics **3**, 24 (2010).

[16] J. Alicea, Phys. Rev. B **81**, 125318 (2010).

[17] A. L. Mackay and H. Terrones, Nature (London) **352**, 762 (1991).

[18] T. Lenosky, X. Gonze, M. Teter, and E. Vert, Nature (London) **355**, 333 (1992).

[19] H. Nishihara and T. Kyotani, Adv. Mater. **24**, 4473 (2012).

[20] M. Kaneda, T. Tsubakiyama, A. Carlsson, Y. Sakamoto, T. Ohsuna, O. Terasaki, S. H. Joo, and R. Ryoo, J. Phys. Chem. B **106**, 1256 (2002).

[21] V. Nicolosi, M. Chhowalla, M. G. Kanatzidis, M. S. Strano, and J. N. Coleman, Science **340**, 1420 (2013).

[22] S. Park, K. Kittimanapun, J. S. Ahn, Y.-K. Kwon, and D. Tománek, J. Phys.: Condens. Matter **22**, 334220 (2010).

[23] S. W. Cranford and M. J. Buehler, Phys. Rev. B **84**, 205451 (2011).

[24] H. Terrones and M. Terrones, New J. Phys. **5**, 126 (2003).

[25] J. M. Soler, E. Artacho, J. D. Gale, A. García, J. Junquera, P. Ordejón, and D. Sánchez-Portal, J. Phys.: Condens. Matter **14**, 2745 (2002).

[26] J. P. Perdew, K. Burke, and M. Ernzerhof, Phys. Rev. Lett. **77**, 3865 (1996).

[27] N. Troullier and J. L. Martins, Phys. Rev. B **43**, 1993 (1991).

[28] E. Artacho, D. Sánchez-Portal, P. Ordejón, A. García, and J. M. Soler, Phys. Status Solidi B **215**, 809 (1999).

[29] H. J. Monkhorst and J. D. Pack, Phys. Rev. B **13**, 5188 (1976).

[30] F. Valencia, A. H. Romero, E. Hernández, M. Terrones, and H. Terrones, New J. Phys. **5**, 123 (2003).

[31] V. M. Pereira, A. H. Castro Neto, and N. M. R. Peres, Phys. Rev. B **80**, 045401 (2009).

[32] A. V. Krasheninnikov, P. O. Lehtinen, A. S. Foster, P. Pyykkö, and R. M. Nieminen, Phys. Rev. Lett. **102**, 126807 (2009).

[33] L.-J. Zhou, Z. F. Hou, and L.-M. Wu, J. Phys. Chem. C **116**, 21780 (2012).

[34] M.-Z. Huang, W. Y. Ching, and T. Lenosky, Phys. Rev. B **47**, 1593 (1993).

[35] K. K. Gomes, W. Mar, W. Ko, F. Guinea, and H. C. Manoharan, Nature (London) **483**, 306 (2012).

[36] M. O'Keeffe, G. B. Adams, and O. F. Sankey, Phys. Rev. Lett. **68**, 2325 (1992).

[37] L. Jiang and Z. Fan, Nanoscale **6**, 1922 (2014).

[38] H. Bi, X. Xie, K. Yin, Y. Zhou, S. Wan, R. S. Ruoff, and L. Sun, J. Mater. Chem. A **2**, 1652 (2014).

[39] D. P. Hashim, N. T. Narayanan, J. M. Romo-Herrera, D. A. Cullen, M. G. Hahm, P. Lezzi, J. R. Suttle, D. Kelkhoff, E. Munoz-Sandoval, S. Ganguli, A. K. Roy, D. J. Smith, R. Vajtai, B. G. Sumpter, V. Meunier, H. Terrones, M. Terrones, and P. M. Ajayan, Sci. Rep. **2**, 363 (2012).

[40] Z. Wang, H. Weng, Q. Wu, X. Dai, and Z. Fang, Phys. Rev. B **88**, 125427 (2013).